Journal of Glaciology, Vol. 36, No. 123, 1990

INSTRUMENTS AND METHODS

DESIGN, DEVELOPMENT, FIELD OBSERVATIONS, AND PRELIMINARY RESULTS OF THE COHERENT ANTARCTIC RADAR DEPTH SOUNDER (CARDS) OF THE UNIVERSITY OF KANSAS, U.S.A.

By G. RAJU, W. XIN, *and* R.K. MOORE

(Radar Systems and Remote Sensing Laboratory, University of Kansas Center for Research, Inc., Lawrence, Kansas 66045-2969, U.S.A.)

ABSTRACT. A modern coherent Antarctic radar depth sounder for probing the ice sheets of Antarctica and Greenland has been designed and developed by the University of Kansas. It was successfully tested during the austral summers of 1987 and 1988 at Downstream B and Upstream B, Antarctica. Ground-based measurements were made with the radar in a mobile hut hauled by a Sno-cat in 1987 and in a Spryte vehicle in 1988.

The coherent Antarctic radar depth sounder (CARDS) is an unfocussed synthetic-aperture chirp radar where the along-track resolution is improved by extensive coherent integration. Surface acoustic wave (SAW) devices are used to implement pulse expansion and compression. A common stable oscillator for the transmitter and the receiver establishes coherency. The system signal-to-noise ratio is enhanced by pulse compression and coherent integration. Antennas for the ground-based measurements are configured with an array of eight dipole elements, four active and four passive, the latter acting as reflectors. The aircraft antennas also consist of four active elements hung underneath the two wings. The wings serve as reflectors. A PC facilitates system control and data recording on a high-density recorder. A-scope plots of selected records allow frequent field checks on system performance. More descriptive display facilities have been incorporated in the latest version of the system.

The radar transmits 60 ns, 20 W peak power at 150 MHz. The number of coherent integrations is selectable up to 64 k. The system is capable of 5 m range resolution and 5 km range in ice. A programmable sensitivity time control (STC) increases the receiver dynamic range. System parameters such as pulse-repetition frequency, number of integrations, and display modes can be chosen during field operations by user-friendly software.

This paper describes the design and field operations of the system. Some results of the 1987 operations at Downstream B are presented.

1. INTRODUCTION

Radars for remote sensing of Antarctica and Greenland have been used since the 1950s (Waite, 1959). There is a continuing need for detailed probing of ice sheets to answer specific questions related to mass balance of and flow from specific ice sheets such as the West Antarctic ice sheet.

VHF radars can determine bottom topography of an ice sheet, give information about the bottom materials, and indicate the presence of layering within the ice sheets that may be an indication both of their history and of potential slippage zones.

The University of Kansas is developing a modern radar at 150 MHz for measurements from a sled, and from a Twin-Otter aircraft. After initial tests, the system may be modified to allow operations on board a C-130 aircraft for continental coverage on a routine basis. The initial Antarctic missions were primarily intended to establish the performance of the system to ensure that it meets the desired scientific objectives.

This is the first Antarctic radio echo-sounder designed completely in the age of solid-state computerized equipment. As a result, it is smaller and more flexible than previous systems. The transmitter uses a low-power solid-state amplifier, so no high voltages are needed. The flexibility attained by complete computer control and signal processing allows the system to be applied to different problems on different vehicles, to attain sensitivity well in excess of that with "brute-force" radars used in the past, and to improve the along-track resolution by synthetic-aperture processing. Once the antennas have been tuned in the field, all control is by entries on the computer keyboard. Because the data are available as digital magnetic records, post-processing for specific applications is possible.

This paper describes the system design, configuration, field operations, and preliminary results for the 150 MHz radar operated both from a mobile hut and a Twin-Otter aircraft. The experiment was carried out during the austral summer of December 1987 in the Downstream B area of Antarctica. During December 1988, measurements at Upstream B were made with the radar mounted in a Spryte tracked vehicle.

2. CHARACTERISTICS OF THE KU RADAR

The system acts as an unfocussed synthetic-aperture radar (SAR) (Ulaby and others, 1982, chapter 9), in which the synthetic-aperture processing is achieved through coherent integration, thereby improving along-track resolution. Coherent integration, pulse addition before detection, is analogous with stacking of seismic signals. Coherent integration also enhances the system signal-to-noise ratio (SNR). Non-coherent integration further improves the apparent SNR. The high peak power needed to overcome the absorption in ice is reduced partly by extensive coherent integration and partly by the chirp technique. Chirp is frequency modulation within a pulse and allows use of a long pulse without sacrificing range resolution.

The choice of an appropriate frequency is constrained by the absorption of the electromagnetic waves in ice. VHF frequencies are preferred since the absorption is smaller at these frequencies than for microwaves, whereas antennas are smaller and resolution can be better than for HF.

2.1. System specifications

The KU radar was designed to achieve a range resolution (in depth) of 5 m in ice and a maximum range of 5 km. In the first two missions, the minimum near range

https://doi.org/10.3189/S0022143000009503 Published online by Cambridge University Press

aimed at was 250 m. Near-surface probing can be easily achieved by by-passing the chirp–dechirp sub-system and retaining the original short pulse.

The main system design problems treated here are:

(a) Obtaining a coherent system.
(b) Pulse expansion, compression, and shaping.
(c) Providing appropriate gains in the receiver to overcome the strong absorption in the ice layers and at the same time implementing time-varying gain control to protect the receiver from saturation by the near-range stronger returns, which is realized by means of a sensitivity time control (STC).
(d) Maintaining good phase linearity at all stages of the system for preserving the pulse shape.
(e) Designing an unfocussed SAR processor that performs both coherent and incoherent integrations in real time.

3. SYSTEM DESIGN

Apart from meeting the desired design goals, emphasis was placed on realizing a modern system with a low transmitter power based on commercially available components and sub-systems. The frequency-modulated chirp technique was chosen for our system after considering several other options from the viewpoint of ease and efficiency. A comparative study of the various chirp techniques such as linear FM using an active source, surface acoustic wave (SAW) dispersive delay lines, and binary phase coding indicated that SAW devices are preferable because of ease of application and performance. Therefore, this technique has been implemented using SAW devices. The specifications of the radar were based on the design considerations described in the following sections.

3.1. Radar equation

The basic radar equation used is

$$P_r = \frac{P_t G^2 \lambda^2 |\Gamma|^2}{(8\pi R_{max})^2 L_a L_s} \qquad (1)$$

where R_{max} is one-way range (depth) in ice = 5 km; G is one-way gain of the antenna = 12 dB in air and 14.5 dB in ice; λ is wavelength; P_t is transmitted power; P_r is received power; B is receiver band width; L_a is two-way absorption loss = 100 dB; L_s is front-end system losses = 3 dB; F is receiver noise figure (from LNA onward) = 2 dB; SNR is signal-to-noise ratio after coherent integration = 0 dB design goal; $|\Gamma|^2$ is power-reflection coefficient = −10 dB (assumed).

This is based on the assumption that the ice layers are essentially reflective, rather than scattering, in Nature. Thus, the power-reflection coefficient is considered instead of the back-scattering coefficient.

An exact value of absorption loss L_a in ice is difficult to estimate because of limited data available in the literature. Hence, because of unknown field conditions, it is often necessary to assume a reasonable figure based on the meager earlier data. We have assumed an average absorption loss of 0.01 dB/m (one-way) (interpolated for −20 °C, from Robin, 1975, fig. 23), considering "cold ice". This is doubtless low for "warmer" ice, but thicknesses are less where ice is warmer, so total loss in these areas may be comparable with that in thick cold ice.

The receiver-noise figure (starting at the input to the low-noise amplifier (LNA)) is assumed to be 2 dB and the SNR after coherent integration is required to be at least 0 dB. The system band width is 17 MHz (approximately the reciprocal of a 60 ns pulse width). Using Equation (1) and the parameters assumed, the equivalent "brute-force" radar transmitter peak power is about 470 kW.

3.2. Range and along-track resolution

For a pulse radar, assuming an average refractive index, n, of 1.78 for the ice (Fletcher, 1970), the range (depth) resolution is given by

$$r_R = \frac{c\tau}{2n} \qquad (2)$$

where c is the speed of light in a vacuum, and τ is the pulse width. For 5 m resolution in ice, τ is 60 ns.

In an unfocussed synthetic-aperture radar, no phase corrections are done (Ulaby and others, 1982); only the part of the synthetic aperture that corresponds to a maximum phase error of $\lambda/4$ is used for determining the ground resolution. The best possible along-track resolution of the unfocussed radar is given by

$$r_{ap} = (R\lambda/2n)^{\frac{1}{2}}. \qquad (3)$$

This is used to determine the limits of pulse-repetition frequency (PRF) and integration samples. The actual resolution depends on the number of integration samples and the altitude and the speed of the platform.

The length of the synthetic aperture is $L = uT$, where u is speed and T is integration time. If we integrate N pulses, $T = N/\mathrm{PRF}$, so $L = uN/\mathrm{PRF}$. On the surface, the along-track resolution is (Moore, 1988)

$$r_a \simeq \lambda R/2L, \text{ or}$$

$$r_a \simeq \lambda R(\mathrm{PRF})/2uN. \qquad (4)$$

For R = 3 km, N = 512, PRF = 4580, and u = 2 m/s, L is 0.223 m, which is so short that the approximate formulas are not applicable. This is not a synthetic aperture and no improvement in resolution results.

The best possible resolution of an unfocussed SAR is given by Equation (3), and is 41 m for R = 3 km. To get this aperture would require 94 k coherent integrations.

In the case of an airborne radar, the antenna beam bends in at the edge of the footprint due to refraction at the air/ice interface. Then, Equation (3) is modified as (Moore, 1988)

$$r_{ap} = (\lambda(h + d)/2n)^{\frac{1}{2}} \qquad (5)$$

where h is the altitude of the aircraft and d is the depth in ice. This becomes 46.7 m for h = 500 m and d = 3 km. For a PRF of 4580 and an aircraft velocity of 80 m/s, r_a will be 244 m. This can be improved to 61 m by increasing N to 2048.

When we are at minimum range, we cannot integrate so many pulses. The best resolution r_{ap} is 22.4 m for a flight altitude of 500 m. Thus, even for the surface echo, a 22.4 m aperture is acceptable. At 4580 PRF, we can integrate 1282 pulses or 2564 at the higher PRF of 9160. We can, therefore, integrate 2048 pulses at the higher PRF and get L = 17.9 m and r_a = 27.9 m, which is close enough to the best possible unfocussed resolution of 22.4 m. This leads to resolutions of 59, 122, and 186 m, at 1, 3, and 5 km depths.

If we integrate longer, the resolution will improve at depth, but the pattern at and near the surface will deteriorate. This occurs because the field pattern is given approximately by a Fresnel integral. If the aperture is too long, the beam widens and eventually separates into multiple beams. This pattern is given by

$$E(y) \approx \int_{-L/2+y}^{L/2+y} e^{-jkx^2/h} dx \qquad (6)$$

where y is the displacement along the track at which we measure the field. The result is

$$E(y) \approx 2[\pi n/k]^{\frac{1}{2}}[F\{(k/h)^{\frac{1}{2}}(L/2 + y)\} - F\{(k/h)^{\frac{1}{2}}(-L/2 + y)\}] \qquad (7)$$

where F is the Fresnel integral. The field pattern is calculated and plotted in Figure 1 for the surface of the ice for different synthetic-aperture (coherent-integration) lengths. It shows that when the aperture is increased to 46.7 m, the pattern splits, leading to an undesirable wider pattern. The resolution is about the same for 17.9 and 22.4 m apertures, and increases to 46 m for a 35.8 m aperture. This shows that the 38.8 m aperture is acceptable for the surface, and one can use it to get better resolution at 3 km (61 m instead

https://doi.org/10.3189/S0022143000009503 Published online by Cambridge University Press

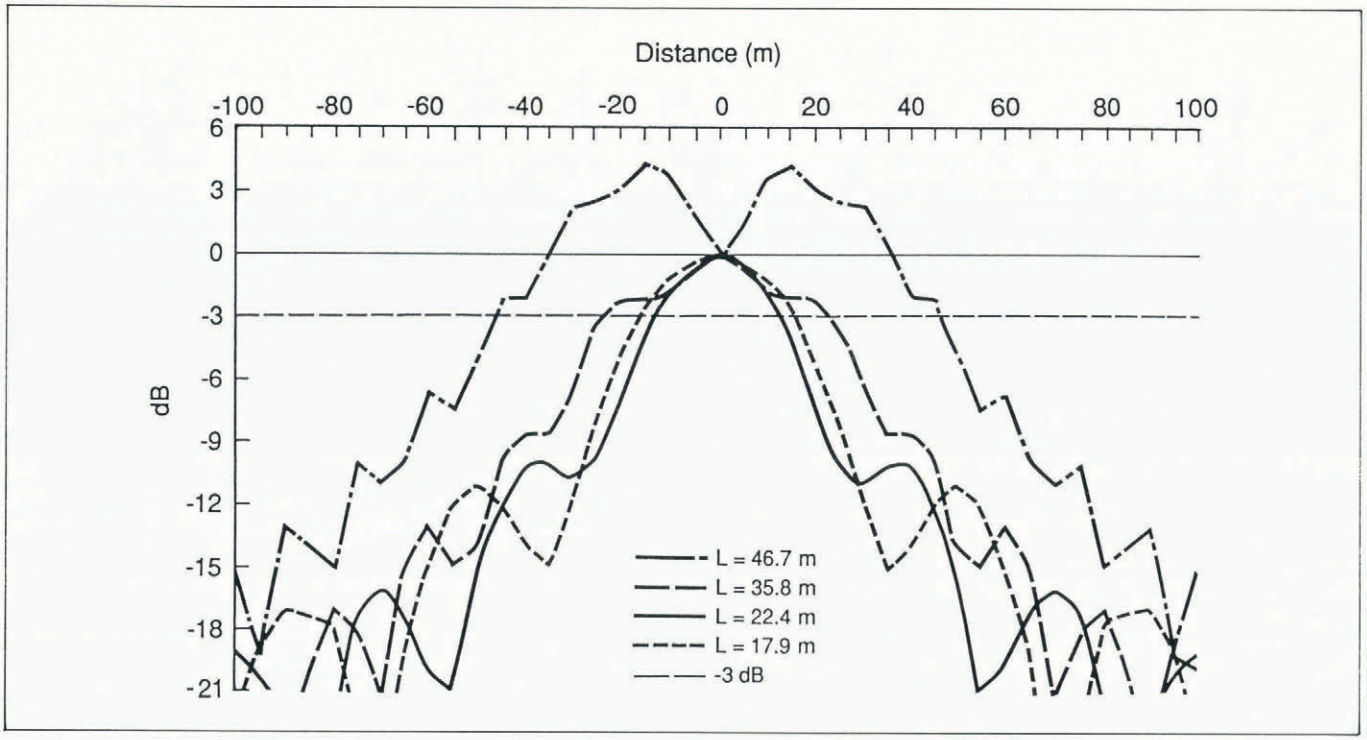

Fig. 1. Patterns of unfocussed SAR.

of 122 m). It requires integration of 4096 pulses at the higher PRF and 2048 at the lower.

3.3. Chirp sub-system

The chirp technique reduces the required peak power by a factor equivalent to the chirp gain. This is defined as the ratio of the expanded pulse length, T, to the original unexpanded pulse length, τ,

$$G_{ch} = \text{chirp gain} = T/\tau. \tag{8}$$

The suitability of commercially available SAW dispersive delay lines for the present chirp sub-system was studied from the viewpoint of center frequency, band width, dispersion time (minimum range), and the capability to operate under severe environmental conditions. The pair most suitable for our system was found to provide an expanded pulse width of 1.6 μs for an input pulse length of 60 ns, resulting in a chirp gain of about 26, thus reducing the peak-power requirement by the same factor. No 15–20 MHz band-width SAW lines were available with suitably short dispersion times. Hence, the SAW expander selected has a band width of 50 MHz and a dispersion time of 5 μs with built-in, Taylor-weighted, range-side-lobe suppression filters. However, our radar used only 17 MHz band width, so the expanded pulse was around 1.6 μs long. The built-in filters were therefore ineffective, and a gating amplifier–attenuator was used to suppress the side lobes.

3.4. Coherent and incoherent integration

The RF power needed for a given signal-to-noise ratio (SNR) can be further reduced, or the SNR of the receiver for a given power can be enhanced, by coherently integrating many received pulses (similar to stacking in seismic work). In the coherent-integration processing, the pulses returned from the target are assumed to be in phase. It can be shown (Ulaby and others, 1982) that the gain for coherent integration of M pulses is

$$G_{co} = (S/N)_{out}/(S/N)_{in} = M. \tag{9}$$

Since the coherent integration increases the SNR by a factor of M, the peak-power requirement is reduced by the same factor.

After coherent integration, the signal is detected and again summed to reduce the noise variance by averaging. This is equivalent to incoherent integration. In this case, samples of the signal being integrated are assumed to be statistically independent samples from a single probability distribution. It can be shown (Ulaby and others, 1982) that the incoherent gain due to Q samples is given by

$$G_{in} = Q^{\frac{1}{2}}. \tag{10}$$

This improves the effective SNR by a factor, G_{in}, once again reducing the needed peak power. The improvement occurs because variances of signal plus noise and noise alone are both reduced by a factor $1/Q$.

If G_{ch} = chirp gain = 1.6 μs/60 ns, G_{co} = coherent gain = programmable (assume 512 samples), and G_{in} = incoherent gain = programmable (assume 16 samples), the peak transmitted power is

$$P_{tc} = \frac{P_t}{G_{ch} \cdot G_{co} \cdot G_{in}} \tag{11}$$

$$= 8.83 \text{ W}.$$

We therefore selected a 20 W transmitter to provide some margin.

3.5. Minimum-detectable range

The length of an expanded pulse constrains the reception of returns from the upper layers since the receiver must be off during transmission, thus restricting the near range. A near-range observation of a few meters may be achieved by by-passing the chirp–dechirp sub-systems, thus converting the chirp radar into a conventional pulse-radar system. The power requirement for such a radar will be quite small since the spreading and absorption losses are much smaller for the near ranges. This modification can be achieved easily, and the radar can be operated in either mode in the field using simple changeover switches. However, because of its implications on other sub-systems such as STC and data processor, this was not attempted for the initial versions.

The expanded pulse width for the chosen expander is about 1.6 μs for an input band width of 17 MHz. This provides a near-range capability of

$$R_{min} = \frac{cT}{2n} = \frac{3 \times 1.6 \times 100}{2 \times 1.78} = 135 \text{ m}. \tag{12}$$

https://doi.org/10.3189/S0022143000009503 Published online by Cambridge University Press

The expanded pulse width of 1.6 μs is at the 3 dB level, but the width at the zero cross-over points is more. Experimentally, it was found that the power is lower by 20 dB at a width of 2.6 μs, leading to R_{min} of 220 m.

When the radar uses separate antennas for the transmitter and the receiver, the strong coupling between the antennas further swamps the near-range returns because of the saturation of the receiver. This effect is less for the airborne system since the receiver recovers from saturation by the time the returns from the surface reach it. A reasonable minimum range is therefore around 250 m.

3.6. Choice of pulse-repetition frequency

The limits on PRF are set by the range, platform speed, along-track resolution, and the unfocussed synthetic-aperture length that is needed. The maximum pulse-repetition frequency is determined by the maximum range expected, R_{max}. From ambiguity considerations, the minimum allowed inter-pulse period is given by

$$T_p = 2R_{max} \cdot n/c. \quad (13)$$

With R_{max} of 5 km and n = refractive index of ice = 1.78, the minimum T_p is 59.3 μs, so the maximum PRF is 16.85 kHz.

Using Equation (3), and with R_{min} (near range) = 250 m and R_{max} = 5000 m, we obtain r_a, the best possible ground resolution for the unfocussed synthetic-aperture case, as 11.85 m and 53 m, respectively. The smaller value of r_a puts a lower limit on the PRF; the time taken to traverse this distance is

$$t = \frac{r_a}{v} = 5.93 \text{ s} \quad (14)$$

where v is the velocity of the sled, considered 2 m/s for the design. The minimum PRF needed is given by

$$\text{PRF} > N/t \quad (15)$$

where N is the number of samples integrated in the coherent integrator. With N = 512 samples, we can have a PRF as low as 87 Hz.

As discussed in section 3.2, the choice of PRF is very important to see if we can get enough integration samples to realize an acceptable synthetic-aperture length for airborne as well as surface operations. Consequently, PRFs of 4580 and 9160 are found to be appropriate for the aircraft operations. For the ground-based operations, a lower PRF is desirable or a very large number of integrations is necessary to get a good along-track resolution. The latest version of the system that has been updated has a higher flexibility in the choice of PRF and number of coherent integrations.

4. SYSTEM CONFIGURATION

Figure 2 shows the block schematic of the overall radar system including the RF and digital sections. The system coherency is established by using a single clock at 9.375 MHz, which is frequency-multiplied to generate the carrier at 150 MHz. It is also used to generate the PRFs and the sampling pulses.

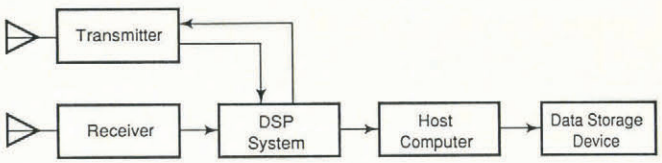

Fig. 2. Block diagram of the overall radar system.

A PC acts as a host computer for the data system. It also controls data recording and display.

The RF section is divided into transmitter and receiver units, each enclosed in a separate shielded box to reduce mutual interference. The block diagram in Figure 3 describes the functional aspects of the various sub-systems of the RF section.

4.1. RF transmitter

The base-band pulse is generated by an impulse generator triggered by the PRF source. The carrier at 150 MHz is generated by multiplying the basic 9.375 MHz clock. The 150 MHz carrier also serves as a coherent local oscillator for the mixer in the receiver. The 60 ns pulse is applied to the carrier in a balanced modulator. The short 150 MHz pulse excites a Surface Acoustic Wave (SAW) dispersive delay line that expands the pulse into a longer pulse of 1.6 μs duration. Since the side-lobe reduction designed for a 50 MHz band width did not work for us, our range side lobes were reduced by means of gating amplifiers and attenuators. The expanded pulse is attenuated by about 48 dB because of the inherently high insertion loss of the SAW devices. It is therefore amplified in an output amplifier, followed by a driver amplifier and then in the final power amplifier to obtain the desired power level of about 20 W.

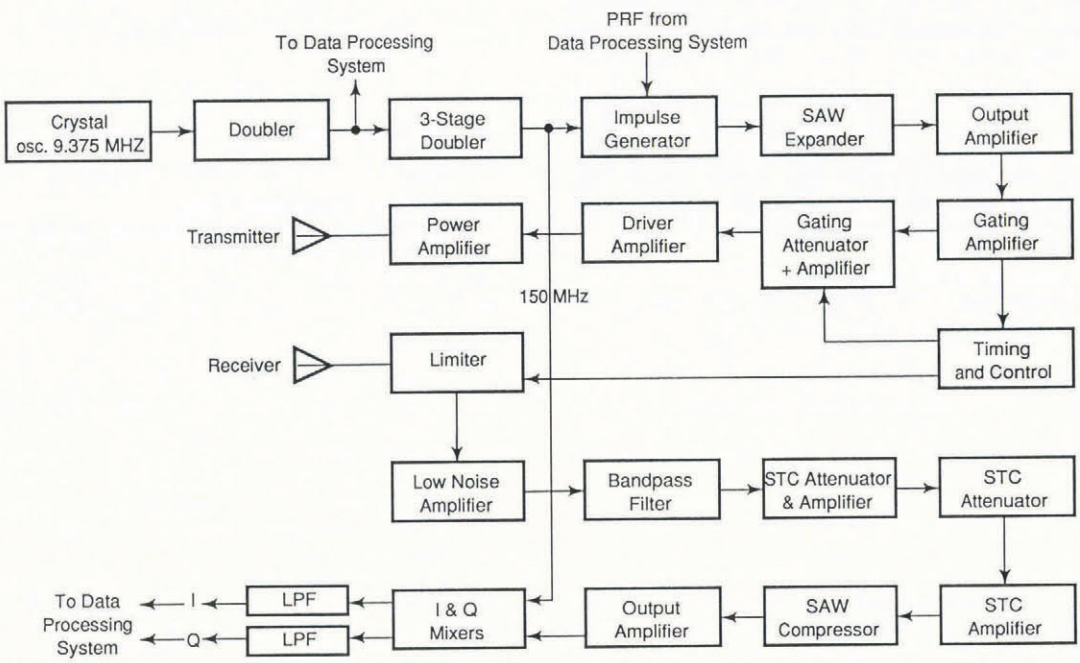

Fig. 3. Functional block diagram of the RF section.

https://doi.org/10.3189/S0022143000009503 Published online by Cambridge University Press

In the earlier system configuration, a PIN-diode duplexer isolated the transmitter and the receiver so that the same antenna could be used for both transmission and reception. In this configuration, although the isolation was reasonably good, the switching transients were found to be too large and seemed to saturate the receiver for a longer duration, thus preventing its operation over useful ranges. Hence, in the field the radar was primarily operated with two antennas. However, a circulator cascaded with a switch in the receiver port was used for a short time to demonstrate the feasibility of the monostatic mode.

4.2. Antennas

The antennas for the ground-based operation consist of a pair of eight-element dipole arrays (West, unpublished), each with four active elements and an equal number of passive elements. Originally, these were designed to operate on a sled, towed behind a Spryte, in which the radar electronics were housed. In the configuration used in December 1987, they hung from a boom across the roof of a mobile hut. In the aircraft version (Xie, 1987), four-element dipole arrays are hung underneath each wing. The metal wings act as the reflectors. The impedances of the antennas are approximately 120 Ω with a small reactive part. This impedance is matched to 50 Ω by using a 77 Ω twin-axial quarter-wave transformer for each element. The transmitter output power is fed to the four antenna elements via a power splitter. A π-network matches antennas to the transmitter and also tunes out the antenna reactance.

4.3. Receiver RF section

A power limiter at the receiver input protects the low-noise amplifier from damage due to high power inputs that might occur because of the large coupling between the antennas. The limiter is more important in the monostatic mode because of the leakage of transmitter power through the T–R circuit.

The receiver should be sensitive enough to respond to the weakest signals echoed from the depth of 5000 m, but at the same time it should be prevented from saturation by the stronger returns from the upper layers of ice. Some sort of a dynamic variation of the sensitivity of the receiver is therefore essential. This is implemented by the STC circuits. The receiver SNR is maintained at an acceptable level at all times by suitably interspersing the gain and attenuation in three stages of about 30 dB each. A set of voltage-controlled attenuators whose control signal is selectable from an EPROM provides this function. This mode provides flexibility in dealing with the often unknown absorption characteristics of ice. The nature of absorption assumed in the design was based upon earlier data (e.g. Robin, 1975). For a specific field situation the best STC setting can be obtained by trial and error (iteration).

To determine the required STC characteristic we apply the radar equation

$$P_r = \frac{P_t G^2 \lambda^2 |\Gamma|^2}{(8\pi R)^2 L_a L_s} \tag{17}$$

where P_t is transmitted power = 43 dB m (20 W); $|\Gamma|^2$ is power reflection coefficient = −10 dB; G is one-way antenna gain = 14.5 dB in ice; L_a is two-way absorption loss = 0.02 dB/m; L_s is system loss = 3 dB; λ is wavelength = 2 m. The attenuation comes from two factors: spreading loss and absorption loss. Assuming that the layers are predominantly reflective, the spreading loss, L_{sp}, is

$$L_{sp} = 1/(8\pi R)^2. \tag{18}$$

The focussing effect in ice can modify L_{sp} to

$$L_{sp} = 1/(8\pi R)^x \tag{19}$$

where x is assumed to be 1.5. More accurate values of x may be determined if the dielectric gradient is known.

The absorptive loss is a function of depth, and it varies from place to place. No definite figures are available for reliably estimating the absorption. However, for the present design, a two-way absorption loss of about 0.02 dB/m (Robin and others, 1975) is considered reasonable. This may be updated as more accurate data become available.

The receiver sensitivity for a single pulse is given by

$$P_{min} = kT_{eff}BF(\text{SNR}) = -99 \text{ dB m} \tag{20}$$

where k is the Boltzmann constant, T_{eff} = 240 K (for ice medium), B = 17 MHz, and F is receiver noise figure = 2 dB. We use SNR = 1, since the eye can detect a pattern in the echoes from successive locations with this low SNR value.

The actual power transmitted is 20 W. If 512 pulses are coherently integrated, SNR per pulse can be as low as −27 dB. The chirp gain, G_{ch} = 14 dB, also contributes to the reduction in required SNR per pulse, so the minimum detectable signal is −140 dB m.

The combined signal and noise level at input of the A/D converter should be maintained within its dynamic range for all levels of the received signal. The signal strength is estimated based on the radar Equation (2). The uncertainties in the parameters used result from possible variations in the density, dielectric constant, composition, and temperature of the various layers of ice. The focussing effect of ice on the propagating waves results in a variation of the spreading loss over different sections of ice. A major factor of concern is the uncertainty in the effect of isolated scatterers.

An efficient system is expected to provide adequate margin for all these uncertainties including fading. In other words, the system should be sensitive enough for the reduced signal level due to the under-estimated losses or should not get saturated because of the higher loss margin provided, as this may cause the signal to fall outside the dynamic range. It is therefore desirable to try to maintain the expected signal level within the operable range of the A/D converter. The STC is expected to meet this requirement. It is programmed with several different gain versus range characteristics to allow for different absorption and spreading losses. The operator may choose the proper one after examining the A-scope display.

After pulse compression, the insertion loss in the compressor is compensated by an output amplifier before it is passed on to the in-phase and quadrature (I and Q) mixers. A sample of the transmitted carrier serves as the reference local oscillator to maintain the phase coherence. A 90° power splitter provides the quadrature references. The mixing process results in a pair of signals (I and Q channels), each with a band width of 8.5 MHz, at a zero "intermediate frequency." This reduces the positive-frequency signal band width by half so the sampling speed of the A/D converters may be lower. The dynamic range of the 8-bit A/D converters is 48 dB. The base-band (zero-IF) pulse is shaped in a pair of linear-phase low-pass filters, which also serve as anti-aliasing filters, and then fed to the A/D converters. Input amplifiers prior to the A/D converters provide the necessary offset and gain to keep the signal at the level acceptable to the A/D converters. To obtain expected SNR improvement by coherent integration, the amplifiers must raise the single-pulse signal level above the 1-bit threshold. This means the noise level is considerably higher since the single-pulse SNR << 1.

4.4. Data-processing section

The block diagram and a flow chart of the data-processing section are shown in Figure 4. It consists of a data-acquisition system, two coherent integrators, one for each channel, a DSP (Digital Signal Processor) sub-system, a host computer, and a mass data-storage system.

With the pipeline structure, all the units of the data system operate in parallel. Communications between any two successive units are accomplished by shared two-port memories. Hardware interrupts are employed for job synchronization between different units. An arbitration circuit was built to solve the common memory-access conflict problem between the DSP sub-system and the host computer. No arbitration circuit is needed at the interface between the coherent integrators and the DSP sub-system, since the data flows only in one direction between these units.

https://doi.org/10.3189/S0022143000009503 Published online by Cambridge University Press

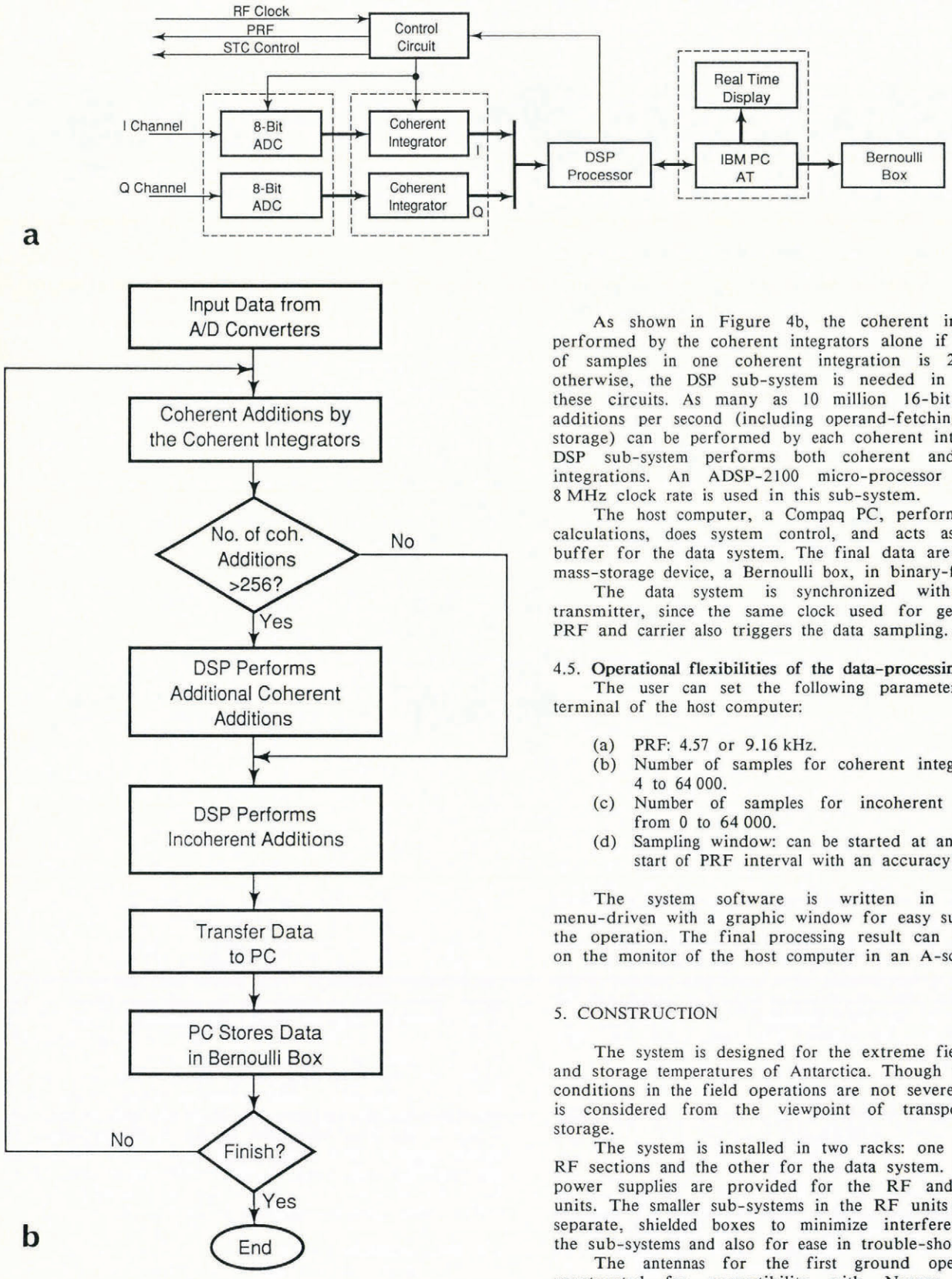

Fig. 4. a. Block diagram of digital section. b. Flow chart of data-processing system.

The base-band signals are sampled in the 8-bit A/D converters at the rate of 18.75 MHz. The length of the sample window is 54.3 μs, which enables 1024 samples from each channel. The start time of the window can be programmed to move to any point within a PRF cycle. Considering the refractive index, n = 1.78 for ice, the window covers up to 4567 m in ice.

As shown in Figure 4b, the coherent integration is performed by the coherent integrators alone if the number of samples in one coherent integration is 256 or less; otherwise, the DSP sub-system is needed in addition to these circuits. As many as 10 million 16-bit fixed-point additions per second (including operand-fetching and data-storage) can be performed by each coherent integrator. The DSP sub-system performs both coherent and incoherent integrations. An ADSP-2100 micro-processor running at 8 MHz clock rate is used in this sub-system.

The host computer, a Compaq PC, performs parameter calculations, does system control, and acts as an output buffer for the data system. The final data are stored in a mass-storage device, a Bernoulli box, in binary-format files.

The data system is synchronized with the radar transmitter, since the same clock used for generating the PRF and carrier also triggers the data sampling.

4.5. Operational flexibilities of the data-processing system

The user can set the following parameters from the terminal of the host computer:

(a) PRF: 4.57 or 9.16 kHz.
(b) Number of samples for coherent integration: from 4 to 64 000.
(c) Number of samples for incoherent integrations: from 0 to 64 000.
(d) Sampling window: can be started at any time after start of PRF interval with an accuracy of 100 ns.

The system software is written in C and is menu-driven with a graphic window for easy supervision of the operation. The final processing result can be displayed on the monitor of the host computer in an A-scope format.

5. CONSTRUCTION

The system is designed for the extreme field operating and storage temperatures of Antarctica. Though the humidity conditions in the field operations are not severe, this factor is considered from the viewpoint of transportation and storage.

The system is installed in two racks: one for the two RF sections and the other for the data system. Separate d.c. power supplies are provided for the RF and the digital units. The smaller sub-systems in the RF units are built in separate, shielded boxes to minimize interference amongst the sub-systems and also for ease in trouble-shooting.

The antennas for the first ground operation were constructed for compatibility with Nansen sleds. The structure was modified in 1987 to suit the mobile hut from which the two antennas were hung. Airborne antennas were based on our electrical design and constructed by Kenn Borek, Canada, U.S. National Science Foundation contractors for airborne Twin-Otter operations in Antarctica.

6. OPERATIONS AND MEASUREMENT RESULTS

6.1. Laboratory tests

Before moving the equipment to the field, the system is tested in the laboratory with dummy loads instead of antennas. This is done by observing the leakage pulse on

https://doi.org/10.3189/S0022143000009503 Published online by Cambridge University Press

the PC monitor after coherent integration. The leakage pulse is a result of insufficient shielding and isolation between the transmitter and the receiver, and is a practical limitation when very weak signals are being measured. The test gives a qualitative check on the system electronics. This test was conducted inside a Jamesway portable building, which had been converted into a semi-permanent laboratory at the Downstream B area, Antarctica.

6.2. Field tests

The antenna was placed on the ice surface outside the laboratory and the matching network was tuned to match the antenna to the transmitter. After the system check, the antenna was integrated with the system and the overall radar was energized for observing the bottom echoes. Strong returns were seen from the bottom and several intermediate layers. After this performance check, the equipment was moved into a mobile hut, "Hilton", for surface-based measurements. Later it was installed in the Twin-Otter aircraft for airborne measurements.

6.3. Ground-based measurements

For conducting the field traverses, the antennas were suspended from a structure attached to the roof of the Hilton. The antennas were close to the ice surface but far enough away to prevent damage. To determine a safe distance, a set of antenna measurements was made for various heights above the surface, and one at a reasonable position and having an acceptable performance was selected. This antenna structure is shown in Figure 5.

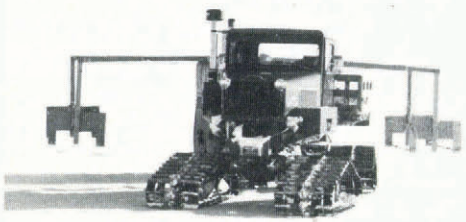

Fig. 5. Radar antennas mounted on the mobile hut, Hilton.

The Hilton is a ski-mounted wooden hut about 6 ft by 7 ft by 8 ft. It is spacious enough to accommodate the radar equipment along with its operators. The system is powered by a 2 kW generator mounted outside the hut, and a power conditioner filters the a.c. power. The hut is pulled by a Tucker Sno-cat. The traverses are run along a marked line, called the z line. Measurements made covered a total distance of about 40 km. The data were acquired over several days of operation. The ground-based operations provided reasonably satisfactory data, but there were some noise problems at times. This was probably attributable to the intense shocks and vibration as the hut was dragged along the rough surface.

6.4. Airborne measurements

After the ground traverses were completed, the system was moved to the Twin-Otter aircraft. The airborne antennas were tuned using matching networks, and the system was integrated with the on-board antennas. Figure 6 shows the antennas as mounted underneath the wings of the Twin-Otter.

Fig. 6. Radar antennas mounted underneath the wings of Twin-Otter aircraft.

The radar was first tested using ground power. After observing the bottom echoes as before, the system was checked using the aircraft power and the inverter. The system was then ready for flight operations.

Because available flight time was limited, only two flights could be made. The first flight was a short one conducted mainly to ensure the overall structural, mechanical, and electrical compatibilty of the radar system with the aircraft. The flight was intended to be along the same z line over which the ground traverses were run. However, due to very poor ground visibility, it was impossible to maintain this track, and the data could not be compared. The performance of the system was satisfactory on this flight.

The second, longer flight involved flying towards the western Antarctic region crossing several defined points as pre-planned. The system performed reasonably well over most of the flight path.

6.5. Measurement results

The data obtained by the measurements made at the Downstream B area are being analyzed. Preliminary results appear in black and white in Figures 7 and 8, and also in color-coded formats. These show several sections of the airborne measurements that are almost spatially continuous. The representations are spatially two-dimensional, with the x-axis corresponding to the distance traveled and the y-axis indicating the depth, after converting the round-trip return

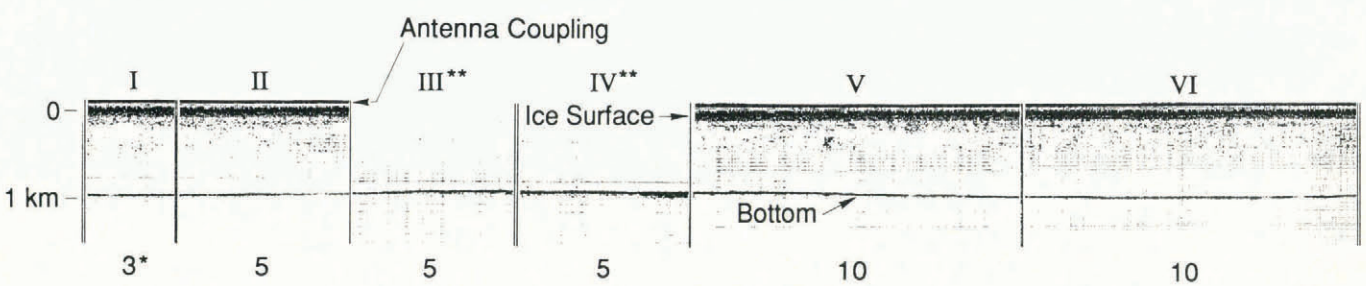

Fig. 7. Results of the first flight operation at Downstream B, Antarctica. Successive data records show contiguous coverage.

https://doi.org/10.3189/S0022143000009503 Published online by Cambridge University Press

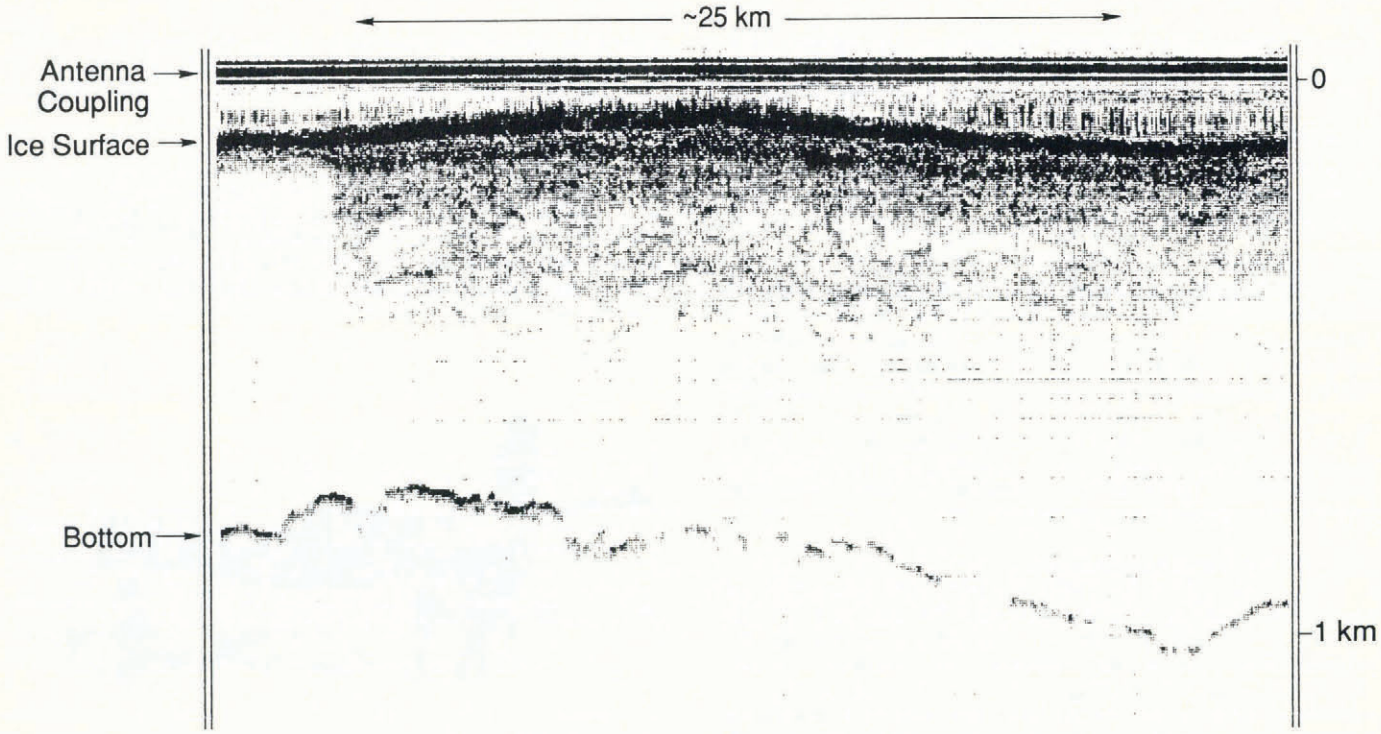

Fig. 8. Sample results of measurements over a crevassed area about 70 miles north-west of DNB (lat. 84°12′ S., long. 154°W.) toward lat. 84°13.4′ S., long. 121°33.2′ W.

time into appropriate distances. The two distance scales are different to enhance the vertical variations. The various gray levels and colors are indicative of the signal strength. The bottom echoes are strong, and several layers appear near the surface. Some of the strong signals near the surface are due to the antenna coupling, and the horizontal lines are noise pulses that can be removed by further processing.

7. CONCLUSION

The satisfactory performance of the system was demonstrated by the results obtained in the Downstream B measurements in Antarctica. It may be necessary to rework parts of the system to improve its reliability for future missions. Particular attention will be given to inter-unit cabling.

8. ACKNOWLEDGEMENTS

This program was supported by a grant from the U.S. National Science Foundation.

REFERENCES

Fletcher, N.H. 1970. *The chemical physics of ice.* Cambridge, Cambridge University Press.

Moore, R.K. 1988. *Coherent integration and resolution.* Lawrence, KS, University of Kansas Center for Research, Inc. Radar Systems and Remote Sensing Laboratory. (RSL Technical Memorandum 8070-1.)

Robin, G. de Q. 1975. Velocity of radio waves in ice by means of a bore-hole interoferometric technique. *J. Glaciol.*, 15(73), 151-159.

Ulaby, F.T., R.K. Moore, and A.K. Fung. 1982. *Microwave remote sensing. II. Radar remote sensing and surface scattering and emission theory.* Reading, MA, Addison-Wesley Publishing Company.

Waite, A.H., *jr.* 1959. Ice depth soundings with ultra-high frequency radio waves in the Arctic and Antarctic, and some observed over-ice altimeter errors. *U.S. Army Signal Res. and Dev. Lab. Tech. Rep.* 2092.

Waite, A.H., *jr.* 1966. International experiment in glacier sounding, 1963 and 1964. *Can. J. Earth Sci.*, 3(6), 887-892.

West, J.C. Unpublished. The design and analysis of an antenna system for use with a coherent Antarctic radar system. (M.S. thesis, University of Kansas, 1986.)

Xie, S. 1987. *The design and construction of a coherent Antarctic radar antenna.* Lawrence, KS, University of Kansas Center for Research, Inc. Radar Systems and Remote Sensing Laboratory. (RSL Technical Memorandum 6810-5.)

MS. received 8 December 1988 and in revised form 19 March 1990